Published in final edited form as:
Sci Transl Med. 2023 May 03; 15(694): eadg3904. doi:10.1126/scitranslmed.adg3904.

Pathophysiology of Dyt1-*Tor1a* dystonia in mice is mediated by spinal neural circuit dysfunction

Amanda M. Pocratsky[1,*], **Filipe Nascimento**[#1], **M. Görkem Özyurt**[#1], **Ian J. White**[3], **Roisin Sullivan**[4], **Benjamin J. O'Callaghan**[4], **Calvin C. Smith**[1], **Sunaina Surana**[1,5], **Marco Beato**[2], **Robert M. Brownstone**[1,*]

[1]Department of Neuromuscular Diseases, UCL Queen Square Institute of Neurology, University College London; London, WC1N 3BG, UK

[2]Department of Neuroscience, Physiology, and Pharmacology, University College London; London, WC1E 6BT, UK

[3]Laboratory for Molecular Cell Biology, University College London; London, WC1E 6BT, UK

[4]Department of Molecular Neuroscience, UCL Queen Square Institute of Neurology, University College London; London, WC1N 3BG, UK

[5]UK Dementia Research Institute, University College London; London, WC1E 6BT, UK

[#] These authors contributed equally to this work.

Abstract

Dystonia, a neurological disorder defined by abnormal postures and disorganised movements, is considered to be a neural circuit disorder with dysfunction arising within and between multiple brain regions. Given that spinal neural circuits constitute the final pathway for motor control, we sought to determine their contribution to this movement disorder. Focusing on the most common inherited form of dystonia in humans, DYT1-*TOR1A*, we generated a conditional knockout of the Torsin Family 1 Member A (*Tor1a)* gene in the mouse spinal cord and dorsal root ganglia (DRG). We found that these mice recapitulated the phenotype of the human condition, developing early onset generalised torsional dystonia. Motor signs emerged early in the mouse hindlimbs before spreading caudo-rostrally to affect the pelvis, trunk, and forelimbs throughout postnatal maturation. Physiologically, these mice bore the hallmark features of dystonia including spontaneous contractions at rest and excessive and disorganised contractions, including co-contractions of antagonist muscle groups, during voluntary movements. Spontaneous

[*]Corresponding authors. a.pocratsky@ucl.ac.uk, r.brownstone@ucl.ac.uk.

Authors contributions:
R.M.B. and A.M.P. conceptualised the project. (R.S. and B.J.O. performed qPCR experiments and formal analysis. S.S. and A.M.P. performed Western blot experiments. I.J.W. performed ultrastructure experiments. A.M.P. performed behaviour experiments. A.M.P., M.G.O., F.N., and C.C.S. performed EMG experiments. A.M.P. performed spontaneous activity and fictive locomotion experiments. A.M.P. performed monosynaptic reflex experiments. M.G.O., F.N., and M.B. performed patch-clamp experiments and formal analysis. M.G.O. and F.N. performed conduction velocity experiments and formal analysis. A.M.P. performed all formal analysis unless otherwise noted. A.M.P. and R.M.B. wrote the original draft of the paper and all authors reviewed, edited, and approved the final manuscript.

Competing interests:
RMB is a co-founder and is on the board of Sania Therapeutics, Inc and consults for Sania Rx Ltd. CCS is an employee of Sania Rx, Ltd.

Europe PMC Funders Author Manuscripts

activity, disorganised motor output, and impaired monosynaptic reflexes, all signs of human dystonia, were recorded from isolated mouse spinal cords from these conditional knockout mice. All components of the monosynaptic reflex arc were affected, including motor neurons. Given that confining the *Tor1a* conditional knockout to DRG did not lead to early onset dystonia, we conclude that the pathophysiological substrate of this mouse model of dystonia lies in spinal neural circuits. Together, these data provide new insights into our current understanding of dystonia pathophysiology.

Introduction

Neural circuits that control movement are distributed across the neuraxis and are comprised of multiple interconnected loops involving the cerebral cortex (1), basal ganglia (2, 3), thalamus (4), cerebellum (5), brain stem (6), and spinal cord (7). Whereas each of these loops has its own function, it is the collaboration of the ensemble that ultimately produces functional movement and hence behaviour. When dysfunction develops within or between these loops, movement disorders arise.

Dystonias are common movement disorders, and are characterised by involuntary sustained muscle contractions across multiple muscle groups, manifesting as abnormal posture and disorganised movements (8, 9). The irregular muscle activity leading to these hallmark postures and movements bears three main neurophysiological signatures: (i) spontaneous muscle contraction at rest (10); (ii) excessive, sustained contractions during voluntary movements often involving co-contractions of antagonistic muscles, which may lead to pain in addition to dysfunctional movement (10, 11); and (iii) altered involuntary sensory-motor reflexes (12, 13). Nonetheless, the neural circuit dysfunction that underlies the pathophysiology of dystonia is not well understood.

The first link between motor control, movement disorders, and the basal ganglia - a cluster of subcortical nuclei - was drawn in the 1600s (14). Thereafter, multiple movement disorders were subsequently classified as basal ganglia syndromes throughout the 1800s and early 1900s, including Parkinson’s disease, Huntington’s disease, and dystonia (15–17). In dystonia, however, limited pathology has been found in the basal ganglia in either humans (18) or animals (19). Moreover, there is a multi-month lag between acquired injury (such as stroke) of the basal ganglia and development of dystonia (20), and a similar lag between deep brain stimulation of the basal ganglia and alleviation of symptoms (21). Furthermore, not all basal ganglia lesions give rise to dystonia (16), and attempts to genetically manipulate basal ganglia nuclei to produce mouse models of dystonia have not been successful (22). To accommodate these findings, dystonia is now commonly considered to be a circuitopathy comprising multiple interconnected brain regions involved in movement, including the basal ganglia, thalamus, cerebellum, and cortex (15).

Ultimately, all output originating from these regions is mediated via motor neurons in the brainstem and spinal cord that send direct projections to muscles to produce coordinated movements. Spinal motor circuits provide key input to motor neurons; these circuits produce and concatenate the basic syllables of limb movement that are disorganised in dystonia: muscle contractions across joints, within limbs, and between limbs (23). Given that the

Europe PMC Funders Author Manuscripts

spinal cord is the final common pathway for motor control and that dystonia is defined by its abnormal muscle contractions and movement disorganisation (10), we sought to determine whether spinal cord dysfunction could be responsible for the pathogenesis of the clinical signs of dystonia.

In this study, we focused on the most prevalent genetic form of dystonia: early onset generalised torsional dystonia, or DYT1-*TOR1A*, which is commonly caused by an in-frame deletion of 3 base pairs in exon 5 of the TorsinA (*TOR1A*) gene (24). We made a mouse model of DYT1-*TOR1A* dystonia that confines *Tor1a* deletion to spinal cord and dorsal root ganglion neurons. We show that these mice develop functional and physiological signs that mirror those seen in human DYT1-*TOR1A* dystonia, and we used these mice to map spinal motor circuit dysfunction. Confining *Tor1a* deletion to dorsal root ganglion neurons did not reproduce the phenotype. We conclude that spinal-restricted deletion of *Tor1a* reproduces the pathophysiology of the human condition.

Results

Restricting *Tor1a* deletion to spinal circuits and dorsal root ganglia

Unravelling the specific contributions of spinal cord dysfunction to movement disorganisation in Dyt1-*Tor1a* dystonia requires site specificity in *Tor1a* deletion: that is, spinal circuits must be directly affected while supraspinal centres are spared. To this end, we used the established Cdx2::FlpO transgenic mouse model as our genetic entry point to manipulating *Tor1a* in spinal circuits as flippase expression is restricted to the developing spinal cord and dorsal root ganglia (DRG) (25). Drawing inspiration from a prevailing Tor1a-flox approach (26–28), we developed a new Tor1a-frt mouse in which exons 3-5 are flanked by frt sites (Fig. 1A; Fig. S1A). Through multigenerational breeding of Tor1a-frt with Cdx2::FlpO mice, we generated a caudal-restricted biallelic “double” conditional knockout (d-cko) of *Tor1a* (Fig. S1B-C). Probing for *Tor1a* and torsinA protein expression in brains, lumbar spinal cords, and DRGs confirmed the site-specificity of this approach. When compared to FlpO-negative littermate controls (Cdx2::wt;Tor1a$^{frt/frt}$), caudal-restricted *Tor1a* d-cko (Cdx2::FlpO;Tor1a$^{frt/frt}$) mice showed normal *Tor1a*-torsinA expression in brain (and heart and liver), but a virtual absence in lumbar spinal cords and DRGs (Fig. 1B-C, Fig. S1D-F), thus validating the site-specificity of our strategy.

Nuclear envelope pathology in Tor1a-deleted spinal and dorsal root ganglia neurons

We next screened for the ultrastructural signature of torsinA dysfunction, nuclear envelope (NE) malformations. Canonical torsinA expression in neurons is distributed throughout the endoplasmic reticulum and NE, but in loss-of-function mutations, torsinA aberrantly accumulates in the NE (29). Morphologically, this can lead to outer nuclear membrane protrusions that balloon into the perinuclear space where they are released as vesicles (27, 30). We found that littermate control spinal neurons had normal, well-defined, closely-apposed nuclear bilayers with occasional nucleoplasmic reticulations decorating the nuclei (Fig. 1D-F, J-K, arrowhead). In contrast, *Tor1a*-deleted lumbar spinal neurons were replete with NE abnormalities. In the dorsal horns, there were groups of spinal neurons that appeared normal (Fig. 1G), exhibited early signs of NE budding with sparse

vesicle accumulation (Fig. 1H), or showed a vesicle-packed perinuclear space with overt separation of the nuclear membranes (Fig. 1I). In contrast, in the ventral horns, almost all spinal neurons screened were affected, with the perinuclear space filled with NE-derived vesicles (Fig. 1L). Multiple vesicles often budded from one protrusion point of the inner nuclear membrane (Fig. 1M) with signs of electron-dense chromatin content filling the vesicles and being released (Fig. 1N). Large area ultrastructural analysis via backscatter scanning electron microscopy of all contiguous spinal neurons embedded within hemicord slices corroborated the ventro-dorsal gradient in NE severity. Of the 2,711 spinal neurons screened in the L4-L5 segments, approximately 60±6% showed ultrastructural abnormalities consistent with torsinA loss of function. In contrast, 8.0±5.0% of the DRG neurons screened in these same segments were affected (Fig. S1H-L, W-Y), suggesting that spinal neurons are particularly vulnerable to *Tor1a* dysfunction. Moreover, ultrastructural screening of basal ganglia neurons did not show aberrant NE budding or vesiculation (Fig. S1M-V). Together, these data confirm that this new mouse model confines the *Tor1a* d-cko to spinal and DRG neurons, with spinal neurons showing ultrastructural signs of torsinA loss-of-function. The model will henceforth be referred to as spinal *Tor1a* d-cko mice.

Spinal-restricted *Tor1a* leads to severe early-onset generalised dystonia

In humans, severe DYT1-*TOR1A* is defined by the early onset, generalised spread of disorganised movements, usually beginning in a lower extremity and then spreading to the trunk and upper limbs (32). The signs stabilize at or below the neck, usually sparing cranial muscle function (33). We discovered similarities between the signs of severe DYT1-*TOR1A* in humans and those in spinal *Tor1a* d-cko mice (Fig. 2A-H). The motor impairments in spinal *Tor1a* d-cko mice emerged early, within the first 1-3 days post-birth, manifesting caudally as hindlimb hyperextension (Fig. 2A; Movie S1). These signs spread bilaterally to affect both lower extremities (Fig. 2B) by postnatal day five (P5). With increasing age, the motor impairments spread rostrally such that by P7-P9 there were clear signs of pelvis, trunk, and forelimb dysfunction, with the forelimbs abnormally extended forward and minimal body weight support (Fig. 2C-D). By P11, the motor signs became fixed at or below the head, sparing orofacial movements. Stepping was impaired as indicated by excessive hindlimb hyperextension with minimal flexion (Fig. 2E). Hindpaw clasping and truncal torsion occurred during tail suspension (Fig. 2F; Movie S2), a test commonly used in Dyt1-*Tor1a* dystonia animal models to uncover latent dystonic-like behaviours (34, 35). By P19-P21, spinal *Tor1a* d-cko mice were severely dystonic with profound abnormal posturing, disorganisation of limb movements (Fig. 2G; Movie S3), and bouts of debilitating truncal torsion (Fig. 2H; Movie S4). Similar to severe DYT1-*TOR1A* in humans, postures were abnormal (Movie S5) and movements were disorganised, jerky, and tremulous in spinal *Tor1a* d-cko mice (Movie S6).

Given that Cdx2::FlpO directs recombination to both spinal and DRG neurons (25), we set out to determine whether *Tor1a* dysfunction confined to DRGs alone (termed “DRG *Tor1a* d-cko mice”) leads to early onset generalised dystonia. Leveraging an analogous multi-generational breeding strategy, we confined the biallelic knockout of *Tor1a* exons 3-5 to DRG neurons using Advillin-cre (36) and Tor1a-flox mice (35). After confirming that *Tor1a* was deleted from DRGs and spared in the spinal cord using qPCR (Table S1),

postnatal video recordings were performed. In contrast to the spinal *Tor1a* d-cko model, DRG *Tor1a* d-cko mice did not develop early onset generalised torsional dystonia (Movie S7). That is, it is Tor1a deletion in the spinal cord that leads to the dystonic phenotype.

After establishing that spinal-restricted *Tor1a* d-cko causes an early onset, generalised movement disorder, we set out to unambiguously define the spatiotemporal window of the dystonic-like phenotype. Five external raters experienced with mouse behaviour were recruited to provide unbiased analyses of postnatal sensory-motor development in littermate controls vs spinal *Tor1a* d-cko mice (Fig. 2I) while blinded to the study design, disease model, mutation, and anticipated motor impairments. Raters assessed postnatal video recordings (P1-P13) and selected - via a unidirectional online test - whether the mouse was a “control” or “mutant,” the latter prompting a follow-up question to select the body regions affected. The unbiased external analysis corroborated our internal findings. At P1, the accuracy rate (proportion of correct observations) in the unbiased detection of spinal *Tor1a* d-cko mice was >60% (Fig. 2J). Throughout postnatal maturation, the accuracy rate steadily increased until it reached 100% at P7 with any subsequent inaccuracy due to false positives (P1-P6: 73% sensitivity, 88% specificity; P7-P13: 100% sensitivity, 98% specificity). A clear spatiotemporal pattern emerged from these unbiased assessments, with motor impairments noted early in the hindlimbs, then spreading rostrally to affect the pelvis, trunk, and forelimbs, with the head minimally affected (Fig. 2K). Thus, *Tor1a* dysfunction confined to spinal circuits causes an overt movement disorder that recapitulates the spatiotemporal motor signs of severe early-onset, generalised dystonia.

The disordered postures and movements observed in severe DYT1-*TOR1A* in humans are defined by (i) persistent involuntary electromyogram (EMG) activity at rest (10) and (ii) disorganised muscle activity during voluntary movements, often including antagonistic co-contractions (10, 11). To test whether the loss of spinal *Tor1a* causes similar aberrant muscle activity signs, we performed acute EMG recordings from the antagonistic tibialis anterior and gastrocnemius hindlimb muscles in pre-weaned wildtype control and spinal *Tor1a* d-cko mice (Fig. 2M).

At rest, there was little to no evidence of spontaneous muscle activity in control mice (Fig. 2M). Conversely, and similar to severe DYT1-*TOR1A* in humans, spinal *Tor1a* d-cko mice had excessive spontaneous activity at rest, including prolonged co-active bursting in antagonist muscles (Fig. 2N; Fig. S2B-C) with few periods of quiescence (Fig. S2A). Indeed, over 90% of the total resting EMG activity was marked by hindlimb muscle activity (Fig. 2O), of which 65% was flexor-extensor co-activation (Fig. 2P) - including co-active single units (Fig. 2N, shaded regions). We also noted episodes of whole hindlimb stiffness associated with co-contractions of ankle extensor-flexor muscles (Fig. S2D-K) and a proximal tremulous-like phenotype (Movie S6), a phenomenon also reported in people with dystonia (11).

Although we were unable to obtain EMG recordings in control neonatal mice given the high level of activity, we leveraged the limited mobility of spinal *Tor1a* d-cko mice to assess EMG activity during tail suspension, a common litmus test for abnormal body posturing in dystonic rodents (34, 35) (Fig. S2L), and volitional locomotion. Tail suspension uncovered

a spectrum of EMG patterns ranging from alternation between flexor-extensor bursting to large amplitude co-contractions, and burst disorganisation between tibialis anterior and gastrocnemius that was interspersed with tonic activity and rhythmic co-contractions (Fig. S2M-Q). During volitional stepping, spinal *Tor1a* d-cko mice showed hindlimb muscle activity with multiple bouts of antagonist co-contractions (Fig. S2R-S). In total, co-contractions of tibialis anterior and gastrocnemius accounted for over one-third of the bursting activity observed during stepping (Fig. S2U). This was clearly an underestimate of the amount of co-activity; when considering single unit coincident activity in addition to the bursts, the proportion of co-contraction time increased (Fig. S2V-W). Disorganised hindlimb muscle activity was further underscored by a considerable range in frequency and duration of bursts (Fig. S2X-Y). Together, these data reveal that spinal-restricted *Tor1a* dysfunction directly leads to an early onset, generalised dystonic-like movement disorder defined by persistent spontaneous muscle activity at rest and excessive co-contractions during rest and voluntary movements.

Excessive, disorganised motor output in mice with spinal deletion of *Tor1a*

We next asked whether *Tor1a*-deleted spinal circuits were the principal source of excessive spontaneous activity and disorganised motor output. Given that the lower extremities are a primary site for disease onset in severe DYT1-*TOR1A* and spinal *Tor1a* d-cko mice, we performed targeted recordings of neural activity intrinsic to the lumbar enlargement - the neural hub for hindlimb motor control (7). Lumbar spinal cords were isolated from P1-P5 mice, thus eliminating the influence of descending systems on spinal motor output and framing the previously-defined window of emerging hindlimb dysfunction. Extracellular electrodes were attached to the caudal and rostral lumbar ventral roots to record electroneurogram (ENG) activity from extensor- and flexor-related spinal motor pools, respectively (37) (Fig. 3A).

In early postnatal isolated spinal cords, there is often spontaneous ENG activity at rest (that is, in the absence of evoked activity), a transient phenomenon that dissipates until little - if any - activity is present by P3-P5 (38), as seen in our littermate controls (Fig. 3B, D). On the other hand, there was spontaneous activity in all isolated spinal cords from P3-P5 spinal *Tor1a* d-cko mice (Fig. 3D). During much of this spontaneous activity, there was co-activation of antagonistic caudal extensor-related (L5) and rostral flexor-related (L2) motor pools (Fig. 3C, shaded inset). These results indicate that the spontaneous activity recorded in the EMGs of spinal *Tor1a* d-cko mice in vivo could result from spontaneous activity in the spinal cord circuits.

Spinal circuits can directly organise and produce rhythmic, coordinated output from flexor-extensor motor pools that manifests as intra- and interlimb movements defining locomotion(*7*). These circuits can be activated in vitro by application of neurotransmitters [N-methyl-D-aspartate, (NMDA), serotonin (5-HT), and dopamine (the latter required for locomotor circuit activation in P3-P5)] to produce a correlate of in vivo locomotion, called fictive locomotion (37), in which rhythmic bursts with an organised flexor-extensor and left-right pattern are produced. In P1-P5 littermate controls during fictive locomotion, stable rhythmic alternation between bilateral flexor-related (rostral lumbar segments, L2), bilateral

extensor-related (caudal lumbar segments, L5), and ipsilateral flexor-extensor related ventral roots was recorded (Fig. 3E, representative of bursting observed throughout P1-P5). In the first 24 hours post-birth, apart from select instances where the normally alternating flexor-extensor activity drifted to synchrony (Fig. 3F, vertical line), spinal motor output in spinal *Tor1a* d-cko mice was largely similar to littermate controls (Fig. S3). But by P2, the previously normal alternating flexor-extensor bursting activity became disorganised (Fig. 3G; Fig. S3), with prolonged bursting at the caudal extensor-related lumbar motor pools, variable burst durations in the rostral flexor-related motor pools, and co-activation between the flexor- and extensor-related spinal motor pools. By P4, ENG bursting was profoundly altered across the lumbar spinal cord (Fig. 3H).

Neural oscillations are defined by their power, frequency, and phase relationship over time. To determine how the spinal *Tor1a* d-cko fundamentally alters neural output, tiered wavelet transformations were used (39). We first isolated the dominant power-frequency bands and cycle durations at individual roots (Fig. S3A-E). We then proceeded with a set of cross-root wavelet transformations to extract the shared power, burst frequency, cycle duration, and phase relationships that define: (a) left-right extensor-related (bilateral caudal roots, L4-L5), (b) left-right flexor-related (bilateral rostral, L1-L2), and (c) ipsilateral flexor-extensor related neural activity. The resultant cross-root convolutions were plotted (Fig. 3I-M) and the dominant (high-power) cross-root burst frequency, cycle duration (Fig. S3), and phase relationships over time were extracted for quantitative analysis of spinal motor output.

Littermate controls showed a consistent dominant high-power frequency band confined to 0.125-0.50 Hz for each root pair assessed (Fig. 3I, M). This power-frequency profile was also observed in spinal *Tor1a* d-cko mice at P1 (Fig. 3J). But by P3 (Fig. 3K), spinal *Tor1a* d-cko mice showed a clear disruption to the power-frequency spectrum with a downward shift in burst frequency such that by P5, the dominant power-frequency band was ~0.016 Hz (Fig. 3L). Extracting the shared frequencies from the high-power bands revealed a decrease in drug-induced burst frequency in all root pairs assessed (Fig. 3N-P). This decrease in burst frequency translated to a ~4-5-fold increase in the cross-root burst cycle duration (Fig. S3F-H).

After establishing the *Tor1a* cko-induced changes to the power-frequency profile, we shifted our focus to cross-root burst coordination, a correlate of the disorganised movements that affect people with dystonia. Cross-root burst coordination data were extracted from the dominant power-frequency bands and plotted on circular graphs wherein 0° denotes in-phase synchrony and 180° reflects out-of-phase alternation.

The classic locomotor profile of out-of-phase bursting activity between bilateral extensors, bilateral flexors, and ipsilateral flexor-extensors (7) was observed in the littermate controls, with phase data concentrated at 180° (Fig. 3Q-S). For the most part, the burst coordination observed in P1 spinal *Tor1a* d-cko mice was broadly similar to littermate controls (Fig. S3L). However, this normal bursting profile became disrupted at P2-P5 wherein there was a predominant shift in the bursting activity towards in-phase synchrony (Fig. 3Q-S). Cross-root coherence remained above 0.8 for all root pairs examined (Fig. S3I-K), suggesting that disruption to rhythmic bursting observed in one root was largely related or predictive

of the disrupted bursting activity observed in the other root. Together, these data reveal that *Tor1a*-deleted spinal circuits directly produce excessive spontaneous activity at rest and disorganised motor output during locomotion.

Spinal monosynaptic reflexes are impaired in spinal *Tor1a* conditional knockouts

Given the spinal locomotor circuit dysfunction, we next looked at the most basic spinal circuit, one that can also be readily studied in humans: the monosynaptic (myotatic) reflex. Case reports indicate that individuals with generalised dystonia, including genetically-confirmed DYT1-*TOR1A*, show diminished monosynaptic reflex amplitudes (12, 40), increased variability in the evoked response amplitude (12, 13), and the infiltration of aberrant asynchronous activity (12). We thus systematically assessed the monosynaptic reflex across the lumbar roots in spinal *Tor1a* d-cko mice (L1-L5) at an age range where the dystonic phenotype was fully penetrant in the hindlimbs (P7-P13).

Graded stimuli of increasing intensity were applied to dorsal roots and the evoked monosynaptic reflexes were recorded from ventral roots (Fig. 4A, bottom). Plotting representative monosynaptic reflexes revealed a spatiotemporal pattern parallel to the dystonic-like phenotype. Compared to age-matched littermate controls, spinal reflexes in *Tor1a* d-cko mice were abnormal in the caudal-most root at P7, but the triphasic waveform appeared normal in the rostral roots (L1, L3) (Fig. 4B). With increasing postnatal age, the impairments to the monosynaptic spinal reflex spread rostrally, affecting L3 and L1 by P11-P13. Examination of the constituent components of the reflex responses (Fig. 4C) revealed that the reflexes in spinal-restricted *Tor1a* d-cko mice had lower amplitudes (Fig. S4F) and longer durations (Fig. 4D-F; Fig. S4G), with multiple asynchronous peaks (Fig. S4A-E). In addition to these impairments in the reflex waveforms, the latency to onset - a measure largely dependent on afferent conduction - was increased in spinal *Tor1a* d-cko mice compared to littermate controls in all segments at all ages (Fig. 4G-I; Fig. S4H). Together, these data suggest that there is a clear caudal-to-rostral progression in monosynaptic spinal reflex impairments during postnatal maturation, including a dispersion of the reflex across time.

Spinal *Tor1a* deletion leads to distributed pathophysiology in the monosynaptic reflex

We next sought to gain mechanistic insights into reflex dysfunction by interrogating the four constituent components of this reflex arc: (a) proprioceptive afferents in the dorsal roots, (b) synapses with motor neurons, (c) the motor neurons themselves, and (d) efferent transmission in the ventral root. We focused on the caudal lumbar motor pools (L4-L5) as they are the earliest affected. We used a ventral horn ablated preparation (Fig. 5A) to determine whether motor neurons were intrinsically affected by the spinal-restricted *Tor1a* deletion. Motor neurons in spinal *Tor1a* d-cko mice appeared smaller than those in littermate controls (Fig. 5B). While motor neurons in spinal *Tor1a* d-cko mice had similar resting membrane potentials as control motor neurons (Fig. 5C), there was a reduction in whole cell capacitance (Fig. 5D; Fig. S5A) and a ~350% increase in input resistance (Fig. 5E; Fig. S5B), consistent with the smaller cell size. Together, these data indicate that lumbar motor neurons are directly affected by *Tor1a* deletion.

But smaller motor neurons alone could not explain all the changes in the monosynaptic reflex, so we next focussed on the afferent limb of the reflex using low-threshold stimulation of the dorsal roots. Compared to littermate controls, afferent-evoked excitatory post-synaptic currents (EPSCs) in spinal *Tor1a* d-cko mice had reduced amplitude, prolonged duration, and multiple asynchronous peaks (Fig. 5F) - outcomes that were corroborated when we activated a subset of afferent fibres via discrete microstimulations (Fig. S5E-G). At all ages assessed, the EPSC area - a measure of charge carried - was decreased in motor neurons in spinal *Tor1a* d-cko mice compared to controls (Fig. 5G; Fig. S5C). There was a decrease in EPSC conductance (Fig. 5H), but when scaled to input conductance there was no difference (Fig. 5I), suggesting that the monosynaptic effects of afferent inputs to motor neurons are similar for littermate control and spinal *Tor1a* d-cko mice. Of note, the total number of boutons expressing vesicular glutamate transporter 1 (vGluT1, a marker for primary afferents) in the ventral horn was reduced (2,470±30 vs 8,280±560 per hemisection; n=2 control, n=3 spinal *Tor1a* d-cko mice at P18), as was the number in close apposition to motor neurons (11±2 vs 25±5 per motor neuron). At all ages tested, there was an increase in the latency to dorsal root-evoked monosynaptic EPSCs in spinal *Tor1a* d-cko mice as compared to controls (Fig. 5J; Fig. S5D), a finding that parallels the increased latencies observed in extracellular recordings.

While the longer latencies could result from impairments at synapses between group Ia afferents and motor neurons, they could also simply be due to deficits in afferent conduction itself. Thus, we recorded L4 and L5 dorsal root volleys in response to root stimulation (Fig. 5K), and found slower afferent conduction velocities in spinal *Tor1a* d-cko mice as compared to controls (Fig. 5L-M), suggesting that the longer latencies to EPSCs resulted from slower conduction velocities. But increased latencies alone cannot account for the asynchronous peaks observed in EPSCs (Fig. S5F). To this end, we microstimulated the dorsal roots at various sites, activating small subsets of fibres whilst recording from the distal root (Fig. 5N-O). After scaling the conduction time by distance, we discovered that spinal *Tor1a* d-cko mice showed longer and variable conduction times as compared to controls (Fig. 5P), suggesting that the multiple peaks in the EPSCs resulted from time dispersion of the incoming afferent action potentials (Fig. S5F-G). That is, two effects occur in the dorsal roots of the spinal *Tor1a* d-cko mice: slower conduction velocities and increased variance of these velocities across fibres.

Given the conduction impairments in dorsal roots, we turned to the ventral roots to determine whether motor axons are also affected (Fig. S5E). We found a decrease in efferent conduction velocity in spinal *Tor1a* d-cko mice as compared to controls (Fig. S5H-J). Responses to microstimulation also revealed increased scaled conduction times and variances in the ventral roots (Fig. S5K-L). In summary, all compartments of the monosynaptic reflex arc - from action potential conduction of sensory afferents to motor neurons to efferent output in the motor roots themselves - are vulnerable to *Tor1a* dysfunction and contribute to impaired sensory-motor integration in *Tor1a* d-cko mice.

Discussion

Our results suggest that spinal circuit dysfunction is a key contributor to the pathophysiology of DYT1-*TOR1A* dystonia. By confining *Tor1a* deletion to the spinal cord and dorsal root ganglion neurons while leaving normal expression in brain, mice phenotypically express a generalised torsional dystonia, have an ultrastructural signature indicating loss of function of torsinA (with unknown relevance to pathophysiology) in spinal but not brain neurons, have spinal locomotor circuit dysfunction, and have abnormal monosynaptic sensorimotor reflexes (27, 30, 31).

Co-existing with the motor impairments were signs of sensory dysfunction, with increased variance in the conduction velocities of the fastest dorsal root fibers in the *Tor1a* d-cko mice. While not a major feature of human DYT1-*TOR1A* dystonia, sensory abnormalities have been reported (41), and sensory tricks - or *gestes antagonistes* - can help to alleviate the symptoms and signs of some dystonias (42). Given that Cdx2::FlpO directs recombinase activity to both spinal and DRG neurons (25), it is reasonable to ask whether the sensory dysfunction observed in spinal *Tor1a* d-cko mice may be due, in part, to the conditional knockout of *Tor1a* in DRG sensory neurons. That said, few DRG neurons showed nuclear envelope malformations. More importantly, confining the *Tor1a* conditional knockout to DRG sensory neurons does not produce early onset generalised torsional dystonia. Together, these data implicate spinal circuits and not primary afferents as the key substrate for dystonia pathophysiology in the spinal *Tor1a* d-cko model.

Our study has limitations. We are reporting a biallelic knockout of *Tor1a*, and human DYT1-*TOR1A* dystonia is largely associated with a mutation in a single allele. Moreover, we were not able to test whether deep brain stimulation (DBS), one of the most effective treatment options for DYT1-*TOR1A* could alleviate dystonic pathophysiology in the spinal Tor1a d-cko model. Testing DBS in spinal *Tor1a* d-cko mice is not technically feasible due to the combination of rapid onset and progression of motor signs in pre-weaned, undersized pups, the size of the necessary hardware, and the expected duration of stimulation needed for alleviation of dystonic signs.

We performed a biallelic knockout of *Tor1a* to unambiguously test our hypothesis that dysfunctional spinal circuits could lead to dystonic pathophysiology, that is, we aimed to produce a phenotypically penetrant mouse model. Whereas children with biallelic *TOR1A* mutations have been identified with increasing frequency (43–44), the vast majority of adults with DYT1-*TOR1A* have a single allele mutation that is associated with reduced penetrance (~30%) and variable phenotypic expression (45). Conversely, the spinal *Tor1a* d-cko mouse model shows complete penetrance: 100% of all the genotype-confirmed biallelic knockouts develop early onset generalised torsional dystonia, suggesting that this model may reflect a more fully penetrant form of the human heterozygote condition. Interestingly, humans with biallelic *TOR1A* mutations have arthrogryposis multiplex congenita 5 (AMC5), which usually includes flexor contractures that present predominantly prenatally or very early postnatally, as well as kyphosis/scoliosis (44). These deformities may be secondary to abnormal neuromuscular activity (46), and as such could potentially result from severe dystonia-related motor neuron activity during foetal development.

Notwithstanding, the spinal *Tor1a* d-cko model is similar to the human monoallelic condition with respect to phenotype and physiology.

Phenotypically, motor signs in the spinal *Tor1a* d-cko mice parallel severe human DYT1-*TOR1A*: dysfunction emerges early in life in a lower extremity and then spreads in a caudo-rostral fashion during developmental maturation until becoming fixed below the head. Thus far, previous rodent models have not reported or recapitulated this pathognomonic feature of DYT1-*TOR1A*, including conditional-ready models wherein *Tor1a* is manipulated in the cortex (35), basal forebrain (47, 48), striatum (28), or cerebellum (49) - key nodes in prevailing models of dystonia (15). Furthermore, in spinal *Tor1a* d-cko mice, the phenotypic signatures of DYT1-*TOR1A* dystonia (abnormal posturing, truncal torsion, and intermittent tremulousness) manifest during naturalistic behaviour when the pups are resting or moving about the environment.

Physiologically, we have shown that spinal *Tor1a* d-cko mice bear the three primary pathophysiological signatures of DYT1-*TOR1A* dystonia: (i) spontaneous muscle contractions at rest (10), (ii) excessive, sustained contractions during voluntary movements (10, 11), and (iii) altered sensory-motor reflexes (12, 13). To date, there has been limited study of the pathophysiological mechanisms underlying these signatures. Equipped with a fully-penetrant mouse model that consistently and reproducibly develops dystonia and a suite of spinal cord preparations to probe sensory-motor dysfunction, we systematically interrogated the precipitating pathophysiological changes of early onset generalised torsional dystonia. Recordings from isolated hindlimb motor neuron pools revealed that excessive spontaneous muscle contractions - including co-activation of motor antagonists - can be directly produced by dysfunctional spinal circuits. Much like the in vivo phenotype, there are clear caudo-rostral generalisations in spinal circuit dysfunction over postnatal development.

The spinal cord is comprised of neural circuits that control the basic syllables of movement, including reciprocal inhibition to change a joint angle, co-excitation of flexor and extensor motor neurons to stabilise a joint, and co-inhibition of these motor neurons to allow the joint to move freely in biomechanical space (50). These syllables are concatenated across time to form functional movement (23). In dystonia, there is abnormal control of these fundamental syllables. akin to a paraphasia of movement. Thus, we pursued the logic that spinal circuit dysfunction could lead to the signs of DYT1-*TOR1A*.

There has been some previous data pointing to spinal circuit dysfunction in dystonia. Dyt1-*Tor1a* animal studies have shown nuclear envelope malformations in spinal neurons (27, 30), spinal motor neuron loss (28), and reduced spinal GABAergic inputs to primary afferent fibres (51). In non-Dyt1 dystonia models, *Lamb1t* mice have coincident EMG activity between opposing muscles, a phenomenon that persists post-spinal transection and thus directly implicates dysfunctional spinal circuits (52). And in people affected by DYT1-*TOR1A*, analyses of spinal reflexes indicate that they may have impairments in monosynaptic stretch reflexes (12, 13) and reciprocal inhibition (10, 53, 54). Even though these reflexes are mediated by spinal circuits, the impairments observed have been attributed to dysfunction of descending systems (53). But spinal circuits are complex, and form

specialised, multi-layered networks that integrate supraspinal, spinal, and sensory inputs to organise motor output (55). Thus, in dystonia pathophysiology, it is logical to consider spinal circuits as a critical nexus for neurological dysfunction and movement disorganisation in dystonia.

We have shown that spinal circuit dysfunction can recapitulate one of the most severe forms of primary dystonia. That is, in the homozygous condition, descending command signals cannot override or compensate for spinal circuit dysfunction such that generalised torsional dystonia manifests over postnatal time. Yet one of the most effective treatment options for DYT1-*TOR1A* is deep brain stimulation (DBS) of a site in the basal ganglia, the globus pallidus internus (56). If spinal circuit dysfunction leads to disorganised movements, then why is DBS an effective treatment for dystonia?

Compared to other DBS-treated movement disorders such as essential tremor or Parkinson's disease, wherein stimulation offers rapid symptom relief within seconds to hours (57), many weeks to months of continuous stimulation is typically required before tonic dystonic movements show improvement (56). (This progressive improvement over months is also seen following pallidotomy) (58). This delay to symptom amelioration could result from neuroplastic mechanisms: a long-term process with adaptive effects that can be localised or distributed via interconnected circuits (57). In fact, maladaptive neuroplasticity is a widely recognised contributing factor to dystonia (59) with mis-wired circuitry implicated in the local motor planning ensemble (basal ganglia loops) (60) as well as distant yet connected circuits such as the corticospinal tract (60). If dystonia-producing maladaptive plasticity is spatio-temporally distributed across remote yet interconnected circuits (including spinal circuits, as shown here), then dystonia-alleviating adaptive plasticity is likely similarly secured. Indeed, evidence for spinal plasticity has been shown: long-term DBS gradually improved spinal-mediated reciprocal inhibition, restoring agonist-antagonist coordination in the forearms of individuals with generalised dystonia (61). That is, it seems likely that DBS-mediated improvement of dystonia involves adaptive plasticity throughout interconnected motor ensembles, including spinal circuits.

That spinal cord circuits have the capacity to adapt is not a new thought (62). Findings over decades of spinal cord injury (SCI) research have established that spinal circuits directly produce organised movements and are intrinsically capable of mediating functional recovery. For example, classic experiments in cats established that following a complete spinal cord transection and resultant paralysis, several weeks of activity-based training can lead to isolated spinal circuits - devoid of descending inputs - to develop the capacity to produce full body weight supported stepping (63, 64). These fundamental studies have been clinically translated: chronic lumbosacral epidural stimulation, paired with activity-based training, can restore function in paralysed humans (65).

To conclude, with this model of DYT1-*TOR1A* dystonia, we have a newfound entry point into investigating the complex pathophysiology of the disease. As a circuitopathy, dystonia can be considered as a process that affects motor circuits throughout the central nervous system, including those in the spinal cord. The notion that spinal motor circuits are simple relays between the brain and muscles has long been dispelled. Yet spinal circuit

dysfunction is rarely considered in movement disorder pathophysiology. We would suggest that new treatment strategies for DYT1-TOR1a dystonia could be aimed at addressing the pathophysiology underlying symptoms, the circuits of which are largely resident in the spinal cord.

Materials And Methods

Study design

The goal of this study was to determine to what extent spinal circuit dysfunction contributes to the pathophysiology of early onset generalised torsional dystonia in mice. Our objectives were to develop and validate a spinal-restricted conditional knockout of *Tor1a*, determine whether spinal circuit dysfunction leads to early onset generalised dystonia, and quantify the extent to which spinal circuit dysfunction contributes to the pathophysiology of this movement disorder.

Experiments were performed in pre-weaned mice with the date of birth recorded as postnatal day 0 (P0). Mice were arbitrarily allocated to the various sets of experiments (qPCR, EMG, ENG) and arbitrarily selected from the litter on a day-by-day basis, randomizing the age of allocation. Experiments were performed blinded to genotype. When blinding was impossible (overt genotype-phenotype), data were collected and coded for subsequent blinded analysis. Due to the nature of this work, *a priori* power analyses were not feasible. Sample sizes were estimated based on our previous experience with each technique. Outliers are shown in the raw data and reported in figure legends. Any data that were excluded from this study are described in the relevant sections.

Animal procedures were approved by the UCL Animal Welfare and Ethical Review Body and carried out in accordance with the Animal (Scientific Procedures) Act (Home Office, United Kingdom, 1986) under project license 70/9098 with experiment metadata reported following the NC3R ARRIVE guidelines. Tor1a-frt mice were generated by Cyagen Biosciences and are made available through the Mutant Mouse Resource and Research Centre (#69706). Additional mice were obtained from the following sources: Cdx2::FlpO (Martyn Goulding, Salk Institute, USA), Advillin-cre (Jax #032536), and Tor1a-flox (Jax #025832).

qPCR

P18 mice (n=14) were anaesthetised and organs harvested for qPCR using probes for *Tor1a*, *Actb*, *Gapdh*, and *Hprt*. *Tor1a* fold expression values were estimated using ΔΔCt method with *Hprt* or *Actb* serving as housekeeping gene.

The same methods were used for quantifying *Tor1a* expression in n=6 P58-P59 littermate control ($Avil^{wt/wt}$;$Tor1a^{wt/flox}$) and n=5 DRG *Tor1a* d-cko mice ($Avil^{wt/cre}$;$Tor1a^{flox/flox}$). Two outliers - one from each group - were excluded from analysis (tissue contamination).

Western blots

P18 mice (n=7) were anaesthetised and organs harvested for Western blot analysis using rabbit anti-torsinA (1:1,000) followed by goat anti-rabbit horseradish peroxidase (HRP)-

conjugated species anti-rabbit secondary antibody (1:1,000). Bands were detected using HRP substrate and imaged for subsequent analysis.

Ultrastructure

P18 (n=8) mice were anaesthetised, transcardially perfused with 0.1M phosphate buffered saline (PBS) followed by 4% paraformaldehyde (PFA). Tissue was harvested and processed for ultrastructure analysis.

Immunohistochemistry

P18 (n=5) mice were anaesthetised and transcardially perfused with 0.1M PBS followed by 4% PFA. Spinal cords were dissected, cryoprotected, embedded, cross-sectioned, and stained with goat anti-choline acetyltransferase (ChAT) (1:250) and guinea pig anti-vGluT1 (1:2,000) followed by donkey anti-goat AlexaFluor-488 (1:1,000) and donkey anti-guinea pig AlexaFluor-647 (1:1,000). Images were acquired and analysed using custom-written scripts.

Behaviour

Mice (n=14) were videotaped (60-90 seconds) starting at P1-P3 and continuing every other day until P14-P15. Five external raters experienced with mouse behaviour were then selected to provide unbiased phenotype scoring.

In vivo electrophysiology

P17 (n=2) and P19 (n=4) spinal *Tor1a* d-cko mice as well as N=4 P18 C57Bl/6J mice were anaesthetised and recording electrodes inserted into the gastrocnemius and tibialis anterior muscles. Recordings were performed with signals amplified, bandpass filtered, digitised, and saved for offline analysis using custom-written scripts.

In vitro electrophysiology: spontaneous activity and drug-induced fictive locomotion

Whole spinal cords were isolated from n=5 P1-P4 littermate controls and n=11 P1-P5 spinal *Tor1a* d-cko pups and transferred to recording chambers perfused with artificial cerebrospinal fluid (aCSF) that was continuously bubbled with 95% O_2/5% CO_2. Recording electrodes were attached to rostral (bilateral L1 or L2) and caudal (bilateral L4 or L5) lumbar ventral roots. Signals were differentially amplified, bandpass filtered, digitised, and saved for offline analysis of spontaneous activity and drug-induced fictive locomotion.

In vitro electrophysiology: monosynaptic reflex

Whole spinal cords were isolated and hemisected from n=24 littermate control and n=21 spinal *Tor1a* d-cko pups aged P7-P13. Spinal cords were transferred to recording chambers perfused with aCSF (bubbled with 95% O_2/5% CO_2). Suction electrodes connected to stimulus isolators were attached to the L1-L5 dorsal roots. L1-L5 ventral roots were attached to extracellular recording electrodes connected to custom-made bipolar electrode holders and headstage-amplifier setup. Motor threshold (MT) was identified for each root after which N=10 sweeps/trial/root were recorded at multiples of threshold. Signals were differentially amplified, bandpass filtered, digitised, and saved for offline analysis.

In vitro electrophysiology: patch-clamp recordings and conduction velocity estimates

Spinal cords were isolated from n=11 littermate control and n=16 spinal *Tor1a* d-cko mice aged P1-P13. Tissue was transferred to recording chamber perfused with aCSF (bubbled with with 95% O_2/5% CO_2). Glass pipettes were pulled, fire polished to a resistance of ~2-4 MΩ, and filled with an intracellular solution. EPSCs were recorded following dorsal root stimulation. Root potentials were recorded following targeted stimulation of different sites along the spinal root. Distances between stimulation and recording sites were recorded to estimate conduction velocities.

Statistical analysis

Statistical analyses were performed using Origin Lab, Microsoft Excel, Data Analysis with Bootstrap-coupled ESTimation Python script, MATLAB, MATLAB-based SpinalCoreN, GraphPad Prism, and SigmaPlot. Differences between groups were considered statistically significant at $p \leq 0.05$. Two-tailed p-values are reported. Outliers (values exceeding average ± 3SD) were excluded from analysis. Descriptive statistics are reported in Table S1.

Supplementary Material

Refer to Web version on PubMed Central for supplementary material.

Acknowledgements

We thank Nadine Simons-Weidenmaier, Rafaela Fernandez De La Fuente, and Hrista Micheva for assisting in animal husbandry, technical support in histology, and beta-testing of scoring system; Kim Dhillon for technical support in image analysis; Stuart Martin for initial genotyping and qPCR support; Kim Dougherty (Drexel University), Shayna Singh (Drexel University), Emily Reedich (University of Rhode Island), Cecilia Badenhorst (University of Calgary), and Monica Gorassini (University of Alberta) for serving as our external raters for unbiased phenotyping. We thank Darlene Burke (University of Louisville) for statistical support, Aharon Lev-Tov (Hebrew University of Jerusalem) for providing the SpinalCore software, Henry Houlden for his molecular support, Martyn Goulding (Salk Institute) for generously providing the Cdx2::FlpO mouse, as well as Tom Warner and Simon Farmer for providing feedback on the manuscript. Thanks to the NVIDIA Corporation for the donation of a Tesla K40 GPU and Quadro RTX 8000. RB is also an honorary consultant neurosurgeon at University College London Hospitals.

Funding

This work was supported by a Wellcome Trust Investigator Grant 110193 (to RMB), Medical Research Council Research Grants MR/V003607/1 (to RMB) and MR/R011494 (to MB and RMB), a Biotechnology and Biological Sciences Research Council Research Grant BB/S005943/1 (to MB), a European Molecular Biology Organisation Long Term Fellowship ALTF 495-2018 (to AMP), a Sir Henry Wellcome Postdoctoral Fellowship 221610/Z/20/Z (to FN), a Royal Society Newton International Fellowship NIF\R1\192316 (to MGO), a Human Frontiers Science Program Long Term Fellowship LT000220/2017-L (to SS), a Medical Research Council Core Funding Grant MC/U12266B (to IJW), a Wellcome Trust Facility Grant 218278/Z/19/Z (to IJW), and a Brain Research UK grant (to RMB)

Data and materials availability

All data associated with this study are in the paper or the supplementary materials. Data are also available at our UCL Research Data Repository (doi: 10.5522/04/c.5922380). Custom-written script for signal analysis is available at Zenodo (https://zenodo.org/record/7818447#.ZDWFyRXMI2U). The *Tor1a-frt* mouse model generated in this study is available from a commercial mouse repository (MMRRC #69706). The Cdx2::Flpo mouse

was obtained from Martyn Goulding (Salk Institute, USA) through a Materials Transfer Agreement.

References

1. Saxena S, Russo AA, Cunningham J, Churchland MM. Motor cortex activity across movement speeds is predicted by network-level strategies for generating muscle activity. Elife. 2022; 11
2. Lee J, Wang W, Sabatini BL. Anatomically segregated basal ganglia pathways allow parallel behavioral modulation. Nat Neurosci. 2020; 23: 1388–1398. [PubMed: 32989293]
3. Klaus A, Silva JAd, Costa RM. What, If, and When to Move: Basal Ganglia Circuits and Self-Paced Action Initiation. 2019; 42: 459–483.
4. MacLean JN, Watson BO, Aaron GB, Yuste R. Internal dynamics determine the cortical response to thalamic stimulation. Neuron. 2005; 48: 811–823. [PubMed: 16337918]
5. Thanawalla AR, Chen AI, Azim E. The Cerebellar Nuclei and Dexterous Limb Movements. Neuroscience. 2020; 450: 168–183. [PubMed: 32652173]
6. Brownstone RM, Chopek JW. Reticulospinal Systems for Tuning Motor Commands. Front Neural Circuits. 2018; 12: 30. [PubMed: 29720934]
7. Kiehn O. Locomotor circuits in the mammalian spinal cord. Annu Rev Neurosci. 2006; 29: 279–306. [PubMed: 16776587]
8. Grütz K, Klein C. Dystonia updates: definition, nomenclature, clinical classification, and etiology. Journal of Neural Transmission. 2021; 128: 395–404. [PubMed: 33604773]
9. Wenning GK, Kiechl S, Seppi K, Müller J, Högl B, Saletu M, Rungger G, Gasperi A, Willeit J, Poewe W. Prevalence of movement disorders in men and women aged 50-89 years (Bruneck Study cohort): a population-based study. The Lancet Neurology. 2005; 4: 815–820. [PubMed: 16297839]
10. Rothwell JC, Obeso JA, Day BL, Marsden CD. Pathophysiology of dystonias. Adv Neurol. 1983; 39: 851–863. [PubMed: 6660125]
11. Cohen LG, Hallett M. Hand cramps: clinical features and electromyographic patterns in a focal dystonia. Neurology. 1988; 38: 1005–1012. [PubMed: 3386815]
12. Novikova VP. Spinal mechanisms of motor disturbances in torsion dystonia (an electromyographic analysis). Neuroscience and behavioral physiology. 1981; 11: 353–357. [PubMed: 7343873]
13. Koelman HTMJ, Willemse RB, Bour LJ, Hilgevoord AAJ, Speelman JD, Visse BWOd. Soleus H-reflex tests in dystonia. Movement Disorders. 1995; 10: 44–50. [PubMed: 7885355]
14. Meyer A, Hierons R. On Thomas Willis's Concepts of Neurophysiology. I Medical history. 1965; 9: 1–15. [PubMed: 14252324]
15. Jinnah HA, Hess EJ. Evolving concepts in the pathogenesis of dystonia. Parkinsonism related disorders. 2017.
16. Neychev VK, Gross RE, Lehericy S, Hess EJ, Jinnah HA. The functional neuroanatomy of dystonia. Neurobiol Dis. 2011; 42: 185–201. [PubMed: 21303695]
17. Newby RE, Thorpe DE, Kempster PA, Alty JE. A History of Dystonia: Ancient to Modern. Movement disorders clinical practice. 2017; 4: 478–485. [PubMed: 28920067]
18. Paudel R, Hardy J, Revesz T, Holton JL, Houlden H. Review: genetics and neuropathology of primary pure dystonia. Neuropathology and applied neurobiology. 2012; 38: 520–534. [PubMed: 22897341]
19. Sharma N, Baxter MG, Petravicz J, Bragg DC, Schienda A, Standaert DG, Breakefield XO. Impaired motor learning in mice expressing torsinA with the DYT1 dystonia mutation. J Neurosci. 2005; 25: 5351–5355. [PubMed: 15930383]
20. Scott BL, Jankovic J. Delayed-onset progressive movement disorders after static brain lesions. Neurology. 1996; 46: 68–74. [PubMed: 8559423]
21. Lozano AM, Hutchison WD, Kalia SK. What Have We Learned About Movement Disorders from Functional. Neurosurgery?. 2017; 40: 453–477.
22. Pappas SS, Leventhal DK, Albin RL, Dauer WT. Mouse models of neurodevelopmental disease of the basal ganglia and associated circuits. Current topics in developmental biology. 2014; 109: 97–169. [PubMed: 24947237]

23. Brownstone RM. Key Steps in the Evolution of Mammalian Movement: A Prolegomenal Essay. Neuroscience. 2020; 450: 135–141. [PubMed: 32446854]
24. Ozelius LJ, Page CE, Klein C, Hewett JW, Mineta M, Leung J, Shalish C, Bressman SB, de Leon D, Brin MF, Fahn S, et al. The TOR1A (DYT1) gene family and its role in early onset torsion dystonia. Genomics. 1999; 62: 377–384. [PubMed: 10644435]
25. Britz O, Zhang J, Grossmann KS, Dyck J, Kim JC, Dymecki S, Gosgnach S, Goulding M. A genetically defined asymmetry underlies the inhibitory control of flexor-extensor locomotor movements. Elife. 2015; 4
26. Pappas SS, Darr K, Holley SM, Cepeda C, Mabrouk OS, Wong J-MT, LeWitt TM, Paudel R, Houlden H, Kennedy RT, Levine MS, et al. Forebrain deletion of the dystonia protein torsinA causes dystonic-like movements and loss of striatal cholinergic neurons. eLife. 2015; 4 e08352 [PubMed: 26052670]
27. Tanabe LM, Liang CC, Dauer WT. Neuronal Nuclear Membrane Budding Occurs during a Developmental Window Modulated by Torsin Paralogs. Cell reports. 2016; 16: 3322–3333. [PubMed: 27653693]
28. Pappas SS, Li J, Le Witt TM, Kim JK, Monani UR, Dauer WT. A cell autonomous torsinA requirement for cholinergic neuron survival and motor control. Elife. 2018; 7
29. Goodchild RE, Dauer WT. Mislocalization to the nuclear envelope: an effect of the dystonia-causing torsinA mutation. Proc Natl Acad Sci U S A. 2004; 101: 847–852. [PubMed: 14711988]
30. Goodchild RE, Kim CE, Dauer WT. Loss of the dystonia-associated protein torsinA selectively disrupts the neuronal nuclear envelope. Neuron. 2005; 48: 923–932. [PubMed: 16364897]
31. Weisheit CE, Dauer WT. A novel conditional knock-in approach defines molecular and circuit effects of the DYT1 dystonia mutation. Hum Mol Genet. 2015; 24: 6459–6472. [PubMed: 26370418]
32. Breakefield XO, Kamm C, Hanson PI. TorsinA: movement at many levels. Neuron. 2001; 31: 9–12. [PubMed: 11498045]
33. Bressman SB, de Leon D, Kramer PL, Ozelius LJ, Brin MF, Greene PE, Fahn S, Breakefield XO, Risch NJ. Dystonia in Ashkenazi Jews: clinical characterization of a founder mutation. Ann Neurol. 1994; 36: 771–777. [PubMed: 7979224]
34. Shashidharan P, Sandu D, Potla U, Armata IA, Walker RH, McNaught KS, Weisz D, Sreenath T, Brin MF, Olanow CW. Transgenic mouse model of early-onset DYT1 dystonia. Human Molecular Genetics. 2004; 14: 125–133. [PubMed: 15548549]
35. Liang CC, Tanabe LM, Jou S, Chi F, Dauer WT. TorsinA hypofunction causes abnormal twisting movements and sensorimotor circuit neurodegeneration. J Clin Invest. 2014; 124: 3080–3092. [PubMed: 24937429]
36. Zhou X, Wang L, Hasegawa H, Amin P, Han BX, Kaneko S, He Y, Wang F. Deletion of PIK3C3/Vps34 in sensory neurons causes rapid neurodegeneration by disrupting the endosomal but not the autophagic pathway. Proc Natl Acad Sci U S A. 2010; 107: 9424–9429. [PubMed: 20439739]
37. Whelan PJ. Developmental Aspects of Spinal Locomotor Function: Insights from Using the in vitro Mouse Spinal Cord Preparation. 2003; 553: 695–706.
38. Bonnot A, Morin D, Viala D. Genesis of spontaneous rhythmic motor patterns in the lumbosacral spinal cord of neonate mouse. Developmental Brain Research. 1998; 108: 89–99. [PubMed: 9693787]
39. Mor Y, Lev-Tov A. Analysis of rhythmic patterns produced by spinal neural networks. J Neurophysiol. 2007; 98: 2807–2817. [PubMed: 17715187]
40. Paudel R, Kiely A, Li A, Lashley T, Bandopadhyay R, Hardy J, Jinnah HA, Bhatia K, Houlden H, Holton JL. Neuropathological features of genetically confirmed DYT1 dystonia: investigating disease-specific inclusions. Acta Neuropathologica Communications. 2014; 2: 159. [PubMed: 25403864]
41. Paracka L, Wegner F, Blahak C, Abdallat M, Saryyeva A, Dressler D, Karst M, Krauss JK. Sensory Alterations in Patients with Isolated Idiopathic Dystonia: An Exploratory Quantitative Sensory Testing Analysis. Frontiers in Neurology. 2017; 8

42. Albanese A, Bhatia K, Bressman SB, Delong MR, Fahn S, Fung VS, Hallett M, Jankovic J, Jinnah HA, Klein C, Lang AE, et al. Phenomenology and classification of dystonia: a consensus update. Mov Disord. 2013; 28: 863–873. [PubMed: 23649720]
43. Kariminejad A, Dahl-Halvarsson M, Ravenscroft G, Afroozan F, Keshavarz E, Goullée H, Davis MR, Faraji Zonooz M, Najmabadi H, Laing NG, Tajsharghi H. TOR1A variants cause a severe arthrogryposis with developmental delay, strabismus and tremor. Brain: a journal of neurology. 2017; 140: 2851–2859. [PubMed: 29053766]
44. Saffari A, Lau T, Tajsharghi H, Karimiani EG, Kariminejad A, Efthymiou S, Zifarelli G, Sultan T, Toosi MB, Sedighzadeh S, Siu VM, et al. The clinical and genetic spectrum of autosomal-recessive TOR1A-related disorders. Brain. 2023.
45. Bressman SB, Sabatti C, Raymond D, de Leon D, Klein C, Kramer PL, Brin MF, Fahn S, Breakefield X, Ozelius LJ, Risch NJ. The DYT1 phenotype and guidelines for diagnostic testing. Neurology. 2000; 54: 1746–1752. [PubMed: 10802779]
46. Kang PB, Lidov HG, David WS, Torres A, Anthony DC, Jones HR, Darras BT. Diagnostic value of electromyography and muscle biopsy in arthrogryposis multiplex congenita. Ann Neurol. 2003; 54: 790–795. [PubMed: 14681888]
47. DeSimone JC, Pappas SS, Febo M, Burciu RG, Shukla P, Colon-Perez LM, Dauer WT, Vaillancourt DE. Forebrain knock-out of torsinA reduces striatal free-water and impairs whole-brain functional connectivity in a symptomatic mouse model of DYT1 dystonia. Neurobiol Dis. 2017; 106: 124–132. [PubMed: 28673740]
48. Berryman D, Barrett J, Liu C, Maugee C, Waldbaum J, Yi D, Xing H, Yokoi F, Saxena S, Li Y. Motor deficit and lack of overt dystonia in Dlx conditional Dyt1 knockout mice. Behav Brain Res. 2023; 439 114221 [PubMed: 36417958]
49. Yokoi F, Dang MT, Li Y. Improved motor performance in Dyt1 ΔGAG heterozygous knock-in mice by cerebellar Purkinje-cell specific Dyt1 conditional knocking-out. Behavioural Brain Research. 2012; 230: 389–398. [PubMed: 22391119]
50. Ronzano R, Lancelin C, Bhumbra GS, Brownstone RM, Beato M. Proximal and distal spinal neurons innervating multiple synergist and antagonist motor pools. Elife. 2021; 10
51. Zhang J, Weinrich JAP, Russ JB, Comer JD, Bommareddy PK, DiCasoli RJ, Wright CVE, Li Y, van Roessel PJ, Kaltschmidt JA. A Role for Dystonia-Associated Genes in Spinal GABAergic Interneuron Circuitry. Cell reports. 2017; 21: 666–678. [PubMed: 29045835]
52. Liu YB, Tewari A, Salameh J, Arystarkhova E, Hampton TG, Brashear A, Ozelius LJ, Khodakhah K, Sweadner KJ. A dystonia-like movement disorder with brain and spinal neuronal defects is caused by mutation of the mouse laminin beta1 subunit, Lamb1. Elife. 2015; 4
53. Nakashima K, Rothwell JC, Day BL, Thompson PD, Shannon K, Marsden CD. Reciprocal inhibition between forearm muscles in patients with writer's cramp and other occupational cramps, symptomatic hemidystonia and hemiparesis due to stroke. Brain. 1989; 112: 681–697. [PubMed: 2731027]
54. Panizza M, Lelli S, Nilsson J, Hallett M. H-reflex recovery curve and reciprocal inhibition of H-reflex in different kinds of dystonia. Neurology. 1990; 40: 824–828. [PubMed: 2330111]
55. Brownstone RM, Bui TV. Spinal interneurons providing input to the final common path during locomotion. Prog Brain Res. 2010; 187: 81–95. [PubMed: 21111202]
56. Krauss JK, Yianni J, Loher TJ, Aziz TZ. Deep brain stimulation for dystonia. J Clin Neurophysiol. 2004; 21: 18–30. [PubMed: 15097291]
57. Herrington TM, Cheng JJ, Eskandar EN. Mechanisms of deep brain stimulation. J Neurophysiol. 2016; 115: 19–38. [PubMed: 26510756]
58. Krack P, Vercueil L. Review of the functional surgical treatment of dystonia. 2001; 8: 389–399.
59. Sherrington CS. Flexion-reflex of the limb, crossed extension-reflex, and reflex stepping and standing. J Physiol. 1910; 40: 28–121. [PubMed: 16993027]
60. Maltese M, Stanic J, Tassone A, Sciamanna G, Ponterio G, Vanni V, Martella G, Imbriani P, Bonsi P, Mercuri NB, Gardoni F, et al. Early structural and functional plasticity alterations in a susceptibility period of DYT1 dystonia mouse striatum. Elife. 2018; 7

61. Tisch S, Limousin P, Rothwell JC, Asselman P, Zrinzo L, Jahanshahi M, Bhatia KP, Hariz MI. Changes in forearm reciprocal inhibition following pallidal stimulation for dystonia. Neurology. 2006; 66: 1091–1093. [PubMed: 16606923]
62. Brownstone RM, Bui TV, Stifani N. Spinal circuits for motor learning. Current Opinion in Neurobiology. 2015; 33: 166–173. [PubMed: 25978563]
63. Forssberg H, Grillner S, Halbertsma J, Rossignol S. The locomotion of the low spinal cat. II Interlimb I coordination. Acta Physiol Scand. 1980; 108: 283–295. [PubMed: 7376923]
64. Barbeau H, Rossignol S. Recovery of locomotion after chronic spinalization in the adult cat. Brain Res. 1987; 412: 84–95. [PubMed: 3607464]
65. Harkema S, Gerasimenko Y, Hodes J, Burdick J, Angeli C, Chen Y, Ferreira C, Willhite A, Rejc E, Grossman RG, Edgerton VR. Effect of epidural stimulation of the lumbosacral spinal cord on voluntary movement, standing, and assisted stepping after motor complete paraplegia: a case study. Lancet. 2011; 377: 1938–1947. [PubMed: 21601270]
66. Deerinck TJ, Bushong EA, Lev-Ram V, Shu X, Tsien RY, Ellisman MH. Enhancing Serial Block-Face Scanning Electron Microscopy to Enable High Resolution 3-D Nanohistology of Cells and Tissues. Microscopy and Microanalysis. 2010; 16: 1138–1139.
67. Fox WM. Reflex-ontogeny and behavioural development of the mouse. Animal Behaviour. 1965; 13 234-IN235 [PubMed: 5835840]
68. Jiang Z, Carlin KP, Brownstone RM. An in vitro functionally mature mouse spinal cord preparation for the study of spinal motor networks. Brain Res. 1999; 816: 493–499. [PubMed: 9878874]
69. Bui TV, Akay T, Loubani O, Hnasko TS, Jessell TM, Brownstone RM. Circuits for grasping: spinal dI3 interneurons mediate cutaneous control of motor behavior. Neuron. 2013; 78: 191–204. [PubMed: 23583114]
70. Özyurt MG, Ojeda-Alonso J, Beato M, Nascimento F. In vitro longitudinal lumbar spinal cord preparations to study sensory and recurrent motor microcircuits of juvenile mice. 2022; 128: 711–726.
71. Dugué GP, Dumoulin A, Triller A, Dieudonné S. Target-dependent use of co-released inhibitory transmitters at central synapses. J Neurosci. 2005; 25: 6490–6498. [PubMed: 16014710]
72. Ho J, Tumkaya T, Aryal S, Choi H, Claridge-Chang A. Moving beyond P values: data analysis with estimation graphics. Nature methods. 2019; 16: 565–566. [PubMed: 31217592]
73. Pocratsky AM, Burke DA, Morehouse JR, Beare JE, Riegler AS, Tsoulfas P, States GJR, Whittemore SR, Magnuson DSK. Reversible silencing of lumbar spinal interneurons unmasks a task-specific network for securing hindlimb alternation. Nat Commun. 2017; 8 1963 [PubMed: 29213073]
74. Pocratsky AM, Shepard CT, Morehouse JR, Burke DA, Riegler AS, Hardin JT, Beare JE, Hainline C, States GJR, Brown BL, Whittemore SR, et al. Long ascending propriospinal neurons provide flexible, context-specific control of interlimb coordination. eLife. 2020; 9 e53565 [PubMed: 32902379]

Europe PMC Funders Author Manuscripts

Europe PMC Funders Author Manuscripts

One Sentence Summary

Deleting Tor1a in the mouse spinal cord leads to severe early onset generalised dystonia, suggesting that spinal dysfunction contributes to the pathophysiology of Dyt1-*Tor1a* dystonia.

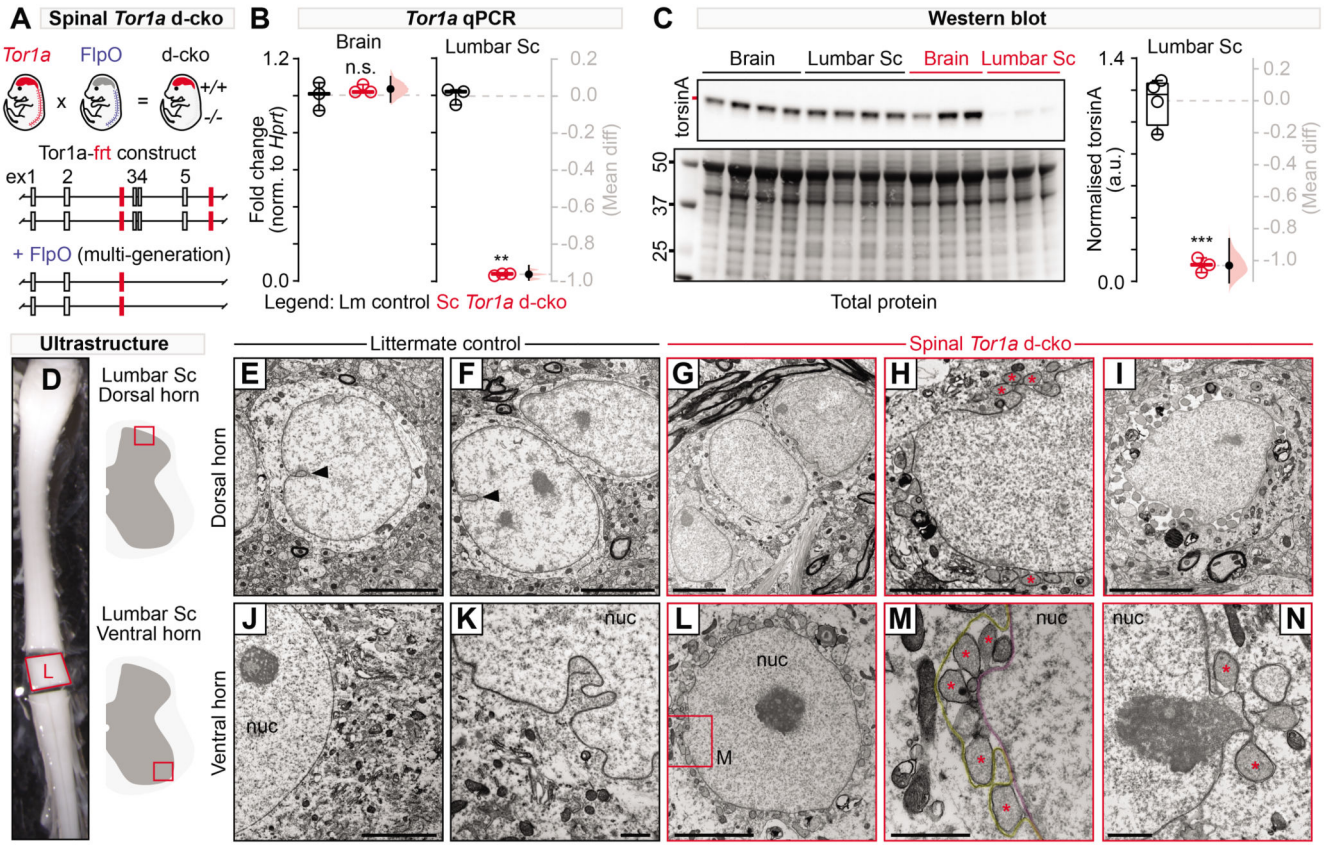

Fig. 1. Characterisation of the spinal-restricted double conditional knockout (d-cko) of *Tor1a*.

(**A**) Shown is a schematic of the genetic strategy used to restrict *Tor1a* deletion to the mouse spinal cord. (**B**) qPCR was used to quantify *Tor1a* expression in brains and lumbar spinal cords of spinal *Tor1a* d-cko mice and littermate controls (***P*<0.001, independent t-test; n=3 P18 control, n=3 P18 spinal *Tor1a* d-cko). (**C**) Western blots are shown for torsin A (~37.5 kD) expression in mouse brains and lumbar spinal cords (****P*<0.0001, n=4 P18 control, n=3 spinal *Tor1a* d-cko). (**D**) Lumbar spinal cords were isolated for ultrastructural analyses of dorsal (**E-I**) and ventral horn (**J-N**) spinal neurons (n=4 P18 control, n=4 spinal *Tor1a* d-cko mice) using electron microscopy. (**E-F**) Dorsal and (**J-K**) ventral horn neurons of littermate controls showed normal nuclear membrane morphology with occasional nuclear invaginations (black arrowhead). Dorsal (**G-I**) and ventral (**L-N**) neurons in spinal *Tor1a* d-cko mice showed nuclear envelope abnormalities, including perinuclear accumulation of vesicles (asterisk) and separation between the inner (**M**, magenta) and outer nuclear membranes (**M**, yellow). "nuc" = nucleus. Scale bars: 5μm (E-J, L), 1μm (K, M-N). Group data are shown (box plots) with individual values overlaid (circles) and mean differences (Gardner-Altman estimation plots). (Also see Table S1, fig. S3).

Europe PMC Funders Author Manuscripts

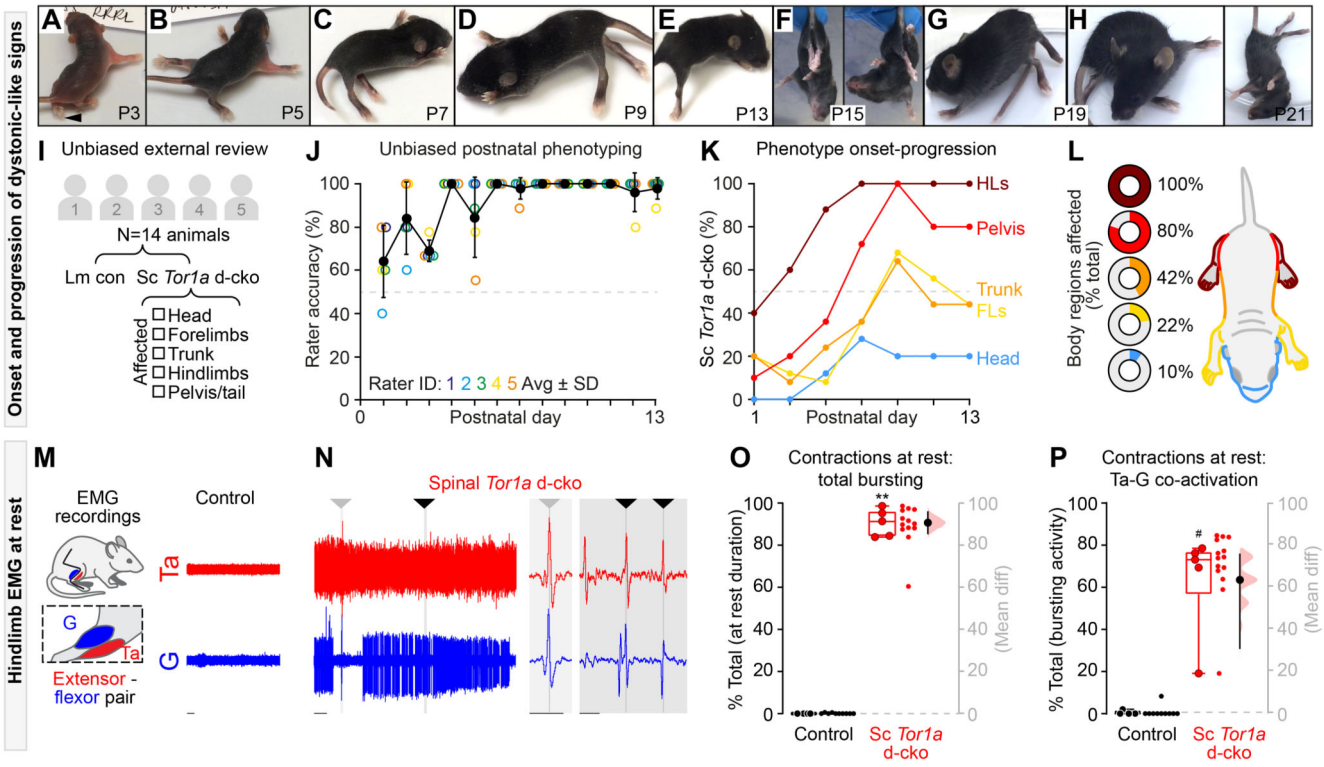

Fig. 2. Spinal-restricted *Tor1a* d-cko leads to early-onset, caudo-rostral progression of movement disorganisation marked by abnormal muscle activity.

(**A**-**H**) Shown are representative still-images of onset-progression of dystonic-like signs in spinal *Tor1a* d-cko mice. (**I**) Experimental design for unbiased external review of phenotype (n=8 control, n=6 spinal *Tor1a* d-cko mice). (**J**) Rater accuracy in identifying genetically confirmed spinal *Tor1a* d-cko mice. (**K**) Spatiotemporal progression of the spinal *Tor1a* d-cko phenotype. (**L**) Depicted are the body regions affected in spinal *Tor1a* d-cko mice. (**M**-**P**) EMG recordings from gastrocnemius (G) and tibialis anterior (Ta) (n=6 P17 and P19 spinal *Tor1a* d-cko mice). (**M**) Representative EMG activity during rest from a P18 wildtype control mouse. (**N**) Spinal *Tor1a* d-cko mice showed excessive spontaneous EMG activity at rest (same amplification as M), including coincident single unit spikes (arrowheads, expanded view in shaded regions). (**O**) Quantification of spontaneous contractions observed at rest (n=4 Control, n=5 spinal *Tor1a* d-cko mice). (**P**) Quantification of Ta-G co-contractions during the at rest spontaneous EMG activity. $^{**}P<0.0001$, independent t-test; $^{\#}P<0.05$, Mann-Whitney U test. Group data shown (box plots) with individual mean values overlaid (circles) and mean differences (estimation plots). Dots: raw data, all at-rest epochs analysed/animal. Scale bars: 1s (M-N), 0.1s (N, shaded regions). (Also see Table S1, fig. S2 and Movies S1–7).

Europe PMC Funders Author Manuscripts

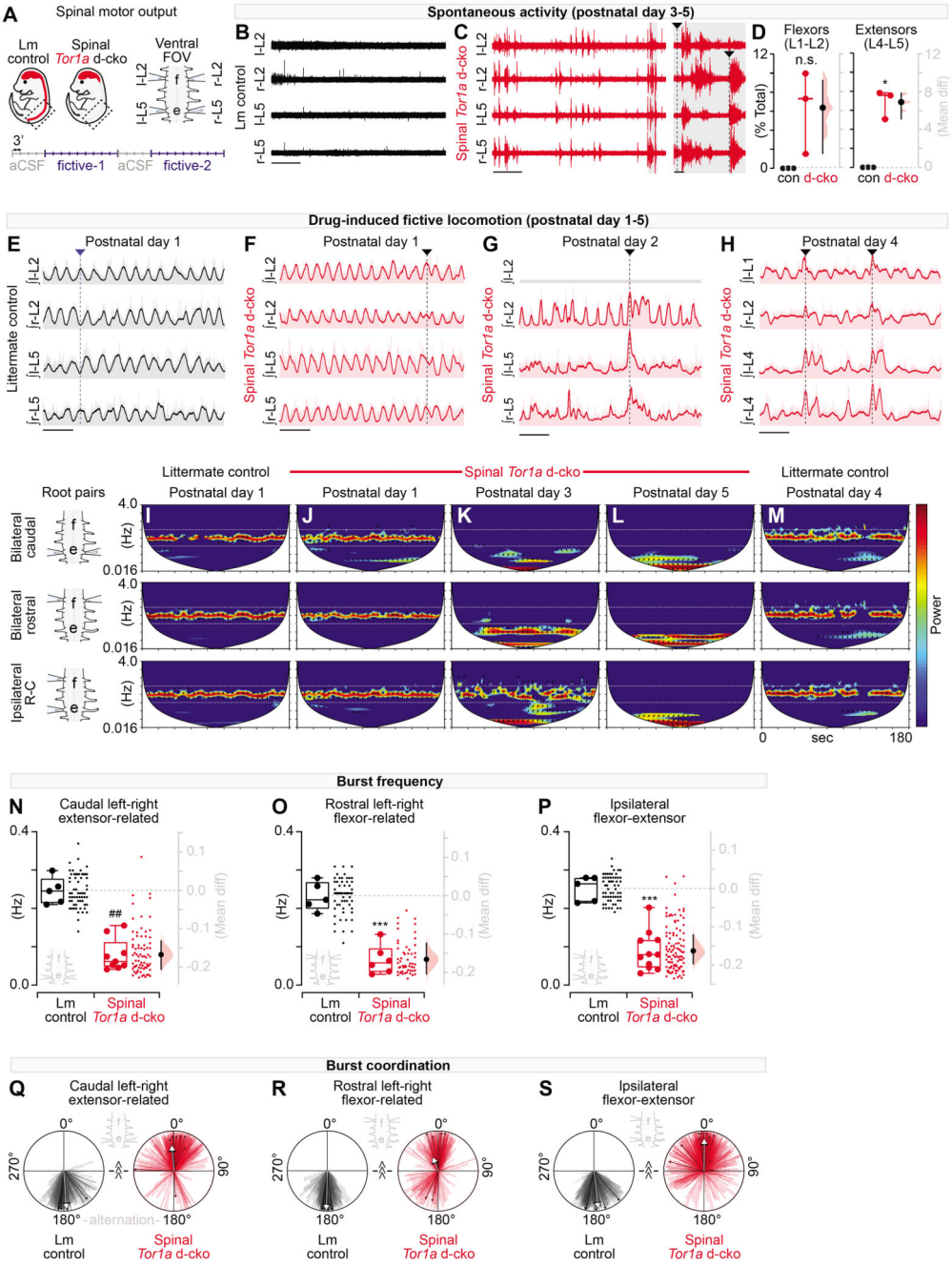

Fig. 3. *Tor1a*-deleted spinal circuits produce excessive spontaneous activity and disorganised motor output.

(**A**) Shown is a schematic of the experimental design for motor output recordings (P1-P5 recordings). (**B-C**) Representative traces (at same amplification) of spontaneous activity at "rest" in artificial cerebrospinal fluid (aCSF). (**D**) Quantification of spontaneous activity (P3-P5: 800-980s per preparation, n=3 control vs n=3 d-cko mice, **P*<0.05, independent t-test with Welch's correction). (**E**) Representative traces of rhythmic, coordinated bursting during drug-induced fictive locomotion in control. Dashed line: alternating bursts at left-

Europe PMC Funders Author Manuscripts

right L2, left-right L5, and ipsilateral L2-L5. (**F-H**) Drug-induced fictive locomotion in spinal *Tor1a* d-cko mice. Dashed lines: burst discoordination. Three channel recording shown in G. (**I-M**) Cross-wavelet analysis of frequency-power (colour, blue-red: 2^7- 2^{13} a.u.) spectrum with phase overlaid (arrows). Horizontal lines: control frequency range. (**N-P**) Quantification of burst frequency in root pairs assessed in spinal *Tor1a* d-cko (n=6-11) vs control (n=5) mice ($^{\#\#}P$=0.001, Mann-Whitney U test; $^{***}P$<0.0001, independent t-test). Group data shown (box plots) with individual mean values overlaid (circles) and mean differences (estimation plots). Dots: raw data, all epochs analysed/animal. (**Q-S**) Quantification of burst coordination ($^{\wedge\wedge\wedge}P$<0.001, Watson's non-parametric U^2 test). Bold arrows, orientation: mean phase, length (0-1): concentration of observations. Group data overlaid onto total observations from all epochs (wedges) and epoch averages (lines). Scale bars: 30s (B-C, left), 10s, (E-H), 1s (C, right). (Also see Table S1 and fig. S3).

Europe PMC Funders Author Manuscripts

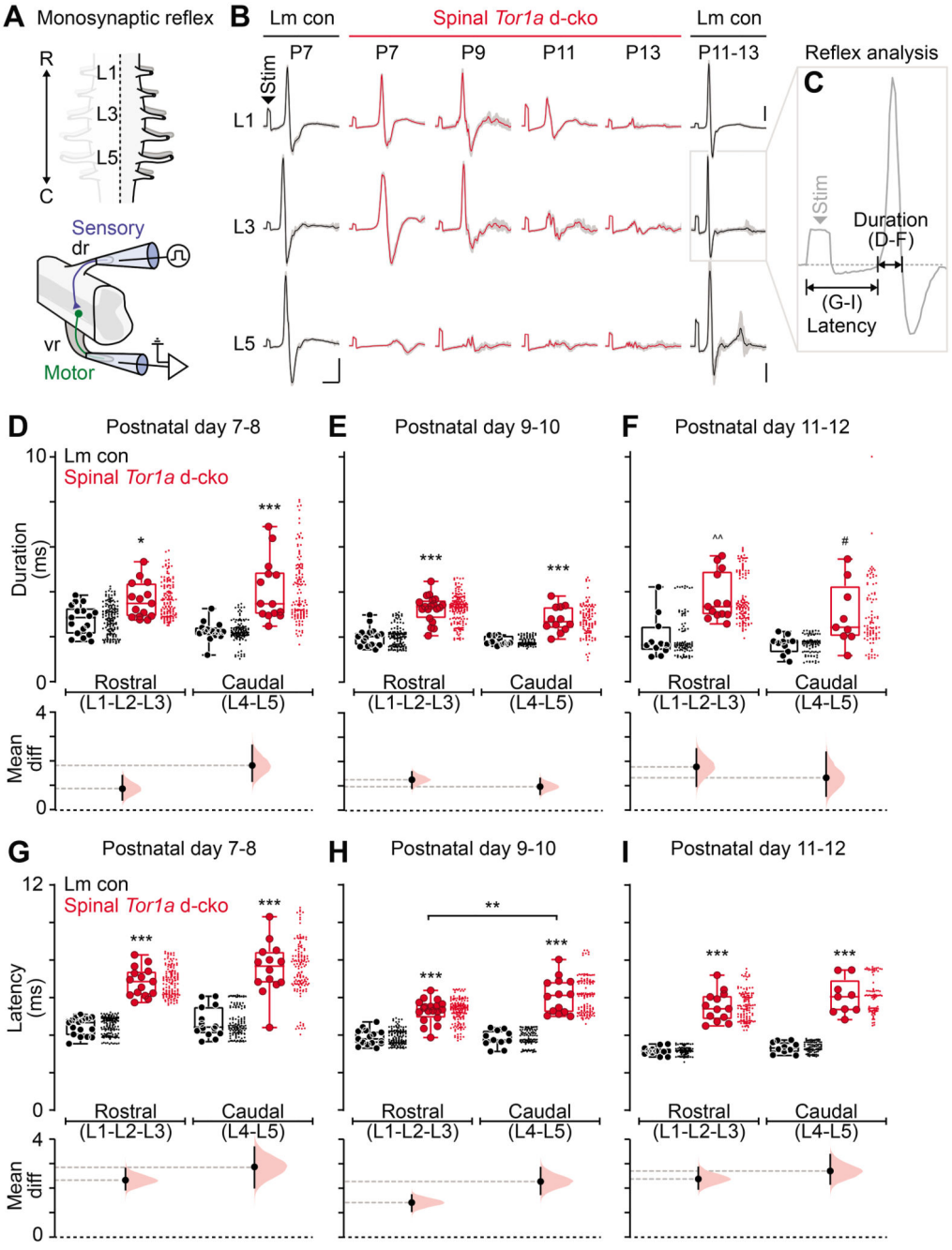

Fig. 4. Spinal-restricted *Tor1a* deletion impairs the monosynaptic reflex.

(**A**) Schematic of the experimental design for recordings of the monosynaptic reflex (P7-P13). (**B**) Representative monosynaptic reflexes at 2.0x threshold. Data shown are average (bold) overlaid onto N=10 sweeps (gray). Scale bars: x=5ms; y=0.05mV. (**C**) Quantification of monosynaptic reflex outcome measures: (**D-F**) response duration and (**G-I**) latency to onset in spinal *Tor1a* d-cko (n=21) vs control (n=24) mice. *P<0.05, **P<0.01, ***P<0.0001, two-way ANOVA and Tukey's *post hoc* t-test; ^^P<0.001, Mann-Whitney U test; $^{\#}P$<0.05, independent t-test with Welch's correction. Group data shown (box plots) with

individual mean values overlaid (circles) and mean differences (estimation plots). Dots: raw data, all reflexes analysed/animal. (Also see Table S1, fig. S4).

Europe PMC Funders Author Manuscripts

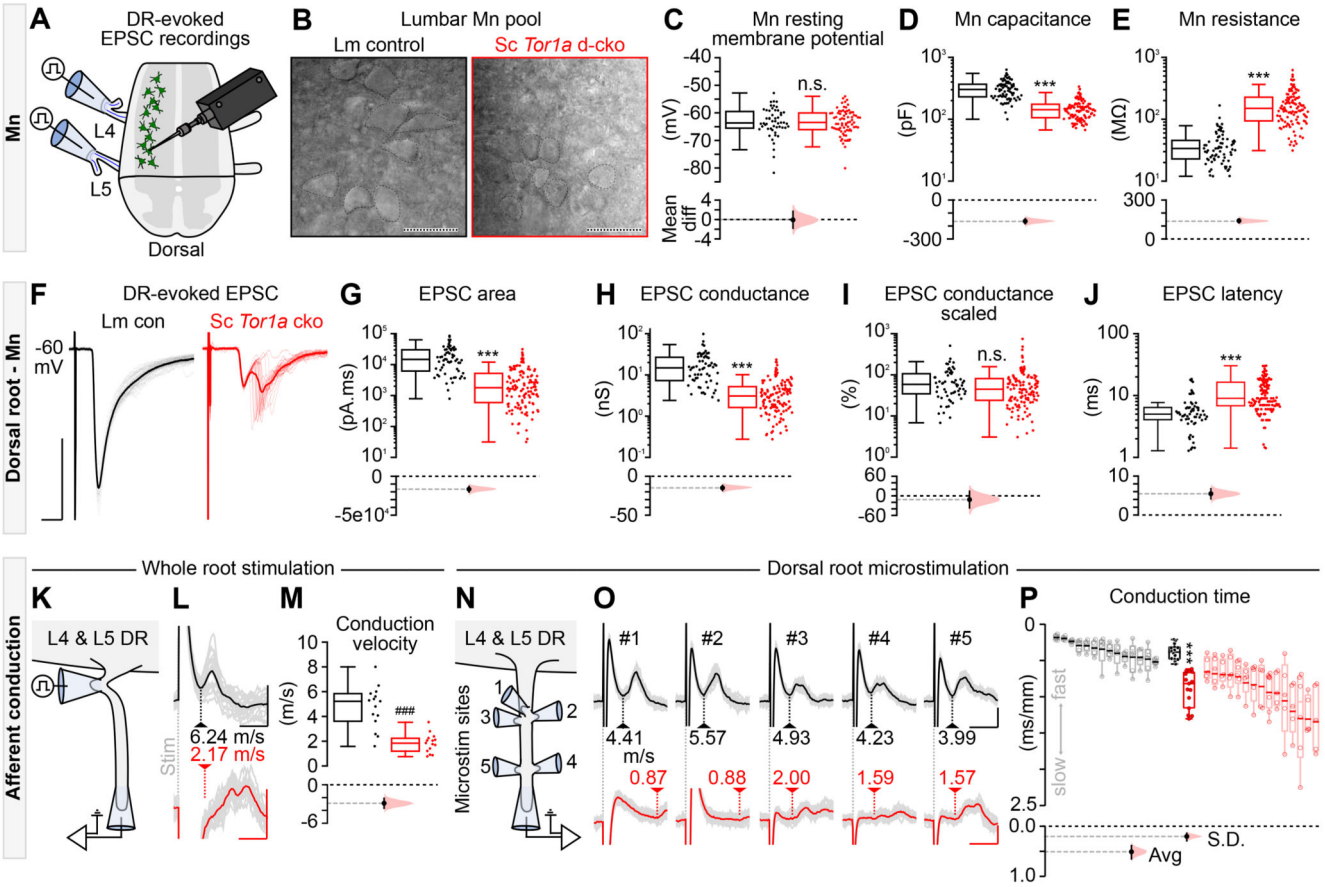

Fig. 5. All components of the monosynaptic reflex are impaired in spinal *Tor1a* d-cko mice

(**A**) Illustration of the experimental design to record afferent- and efferent-evoked excitatory post-synaptic potentials (EPSCs). (**B**) Differential interference contrast (DIC) images of P9 motor neurons (scale bars: 50μm). Quantification of intrinsic properties (P1-P13 n=# of motor neurons): (**C**) resting membrane potential (n=52 vs n=77, P=0.68, Mann-Whitney U test), (**D**) whole cell capacitance (n=73 vs n=108, ***P<0.0001, Mann-Whitney U test), and (**E**) input resistance (n=73 vs n=111). (**F**) Representative example, P7 dorsal root (DR)-evoked EPSC. Scale bars: x=5ms, y=500pA. Quantification of DR-evoked EPSCs: (**G**) area (n=61 vs n=130), (**H**) absolute conductance (n=61 vs n=128), (**I**) scaled conductance (n=61 vs n=126, P=0.06), and (**J**) latency (n=60 vs n=131) (P1-P13). Group data shown (box plots) with mean differences (estimation plots). Dots: raw data, all responses analysed/animal. (**K**) DR stimulation to estimate afferent conduction velocity. (**L**) Representative afferent volleys following whole root stimulation at threshold. Scale bars: x=0.5ms, y=0.05mV (black) or 0.025mV (red) (L5 DR in P8 control and P6 spinal *Tor1a* d-cko mice). (**M**) Quantification of L4 & L5 DR conduction velocity (P6-P10 n=15 vs n=15, ###P<0.0001; independent t-test). (**N-O**) Representative examples of DR microstimulation afferent conduction velocities in control (black, scale bars: x=0.5ms, y=0.05mV) and spinal *Tor1a* d-cko mice (red, scale bars: x=3ms, y=0.025mV). (**P**) Quantification of afferent conduction time (P6-P10, n=14 vs n=15 mice, Avg: ***P<0.0001) and variance (S.D.: ***P<0.0001). Averaged data shown in black and red box plots with individual mean values (within each root) overlaid (filled

Europe PMC Funders Author Manuscripts

circles) and mean differences (estimation plots). The responses from individual roots - including raw (open circles) and averaged (bold line) values - are shown as de-saturated box plots adjacent to the averaged dataset. (Also see Table S1, fig. S5).

Europe PMC Funders Author Manuscripts